COVER SHEET

ADIABATIC NANO-FOCUSING OF PLASMONS BY SHARP METALLIC WEDGES.

Dmitri K. Gramotnev and Kristy C. Vernon

Applied Optics Program, School of Physical and Chemical Sciences,

Queensland University of Technology, GPO Box 2434, Brisbane, QLD 4001, Australia.

Fax: (+61 7)3864 2584

Email: d.gramotnev@qut.edu.au, k.vernon@qut.edu.au

ABSTRACT

This paper demonstrates the possibility of efficient adiabatic nano-focusing of plasmons by a sharp triangular metal wedge. Geometrical optics approach and the approximation of continuous electrodynamics are used for the analysis. In particular, it is demonstrated that both the phase and group velocities of an incident anti-symmetric (with respect to the magnetic field) plasmon tend to zero at the tip of the wedge, and the plasmon adiabatically slows down, eventually dissipating in the metal. Typically, the amplitude of the plasmon significantly increases near the wedge tip, but this increase is finite even in the absence of dissipation in the metal. The dependence of the local field enhancement near the tip on structural parameters, dissipation in the metal, angle of incidence, etc. is analyzed in this paper. It is also shown that an anti-symmetric film plasmon can effectively be guided by a triangular metal wedge, forming a wedge plasmon mode that is localized near the tip of the wedge and propagates along this tip. A new existence condition for these localized wedge plasmons is derived and discussed.

PACS codes: 78.67.–n; 68.37.Uv; 73.20.Mf

1. Introduction

Nano-focusing of light is localization of electromagnetic energy in regions with dimensions that are significantly smaller than the wavelength. This is one of the central problems of modern near-field optical microscopy that takes the resolution of optical imaging beyond the diffraction limit of light [1-14]. It is also important for the development of new optical sensors and delivery of strongly localized photons to tested molecules/atoms (e.g., for local spectroscopic measurements [13-19]). Nano-focusing is also one of the major tools for efficient coupling of light and light-carried information into sub-wavelength waveguides, interconnectors and nano-optical devices [20].

One of the most common approaches to nano-focusing of light is based on the use of strongly localized surface plasmons in metallic nano-structures, such as sharp metal tips [7,10,14], dielectric conical tips covered with metal film [4,11-13], conical and pyramidal tips covered in metal film with nano-aperture [9,12,21-24], etc. These are the structures commonly used in scanning near-field optical microscopy. In addition, nano-focusing of plasmons in metallic nano-structures is usually accompanied by strong enhancement of local electromagnetic field, especially near sharp metallic tips and dielectric tips covered with metal [4,7,10,13,14]. This provides an interesting opportunity to develop new optical sensors based on the local field enhancement. For example, several papers have reported Raman spectroscopy from molecules near a sharp metal tip with nano-focusing [14-18]. Thus, strong enhancement of the local field that can be achieved during nano-focusing [7,10,14,20] may be used for possible development of new SERS sensors capable of single molecule detection with sub-wavelength resolution (if used in combination with a scanning near-field optical microscope).

Nano-focusing of plasmons by means of nano-tips is analogous to a spherical lens, because in both these cases the electromagnetic energy is focused into a region localized in two dimensions (like a circular spot). However, in the case of a spherical lens, this region cannot be smaller than half-the-wavelength of the focused radiation (the diffraction limit of light), while for a metallic nano-tip, the region of localization may be arbitrarily small (in the approximation of the continuous electrodynamics and absence of dissipation in the metal) [7,10,14]. Similarly, nano-focusing of plasmons by metallic wedges and V-grooves [20,25] should be analogous to a conventional cylindrical lens, because these structures focus the light into regions that are localized only in one direction (like a thin strip). The minimal width of this strip for a conventional cylindrical lens is limited by half-the-wavelength in the medium, while for nano-focusing by a metallic groove this strip can be arbitrarily narrow (in the approximation of the continuous electrodynamics) [20].

Theoretical analysis of nano-focusing of plasmons by a sharp groove was conducted in the geometrical optics approximation (GOA) [20] and using the approximate solution in the cylindrical coordinates [25]. The analysis conducted in [25] is also directly applicable for the investigation of nano-focusing by sharp metal wedges. However, the applicability of this method is highly restrictive, so that the developed approximate theory is valid only in the close proximity (typically, within a few tens of nanometers) of the tip of the wedge/groove [25]. The applicability conditions for the GOA approach are much less restrictive, and it is usually applicable for a much broader range of structural parameters [20]. However, the conducted analysis based on GOA [20] was limited only to nano-focusing in metallic grooves. No detailed investigation of plasmon propagation and nano-focusing in sharp metallic wedges has been conducted so-far.

Therefore, the aim of this paper is to develop a theory of nano-focusing of strongly localized plasmons by a sharp metal wedge in the geometrical optics (adiabatic) approximation. In particular, it will be demonstrated that only plasmons with anti-symmetric distribution of the magnetic field across the wedge will experience nano-focusing with their phase and group velocities asymptotically tending to zero as the plasmon approaches the tip of the wedge. The effect of dissipation in the metal will be investigated in detail, and the optimization of structural parameters will be described. Some important applicability conditions for strongly localized wedge plasmons [26] guided by the tip of a wedge will also be determined and discussed. Comparison with the plasmons in sharp V-grooves will be carried out.

2. Geometrical Optics Approximation

Consider an infinite metal wedge with the angle γ and complex permittivity $\varepsilon_2 = e_1 + ie_2$ ($e_1 < 0$, $e_2 > 0$), surrounded by a dielectric medium with real and positive dielectric permittivity ε_1, such that $|e_1| > \varepsilon_1$ (the existence condition for surface and film plasmons [27,28]). The angle of the wedge is assumed to be sufficiently small (the specific conditions restricting the wedge angle are presented below). The coordinate axes are as indicated in the figure.

Consider two surface plasmons of the same frequency on the opposite sides of the wedge, both propagating towards the tip of the wedge at the same angle of incidence θ with respect to the *y*-axis. At a large distance from the tip of the wedge, where these plasmons can be regarded uncoupled, the angle of incidence is equal to θ_0 (Fig. 1b). As the two plasmons travel towards the tip of the wedge, the thickness of the wedge decreases, and the plasmons couple across the wedge. The wedge is effectively a metal

film (membrane) with varying thickness. Therefore, the coupled plasmons form a film plasmon.

There are two types of film plasmon – with the symmetric and anti-symmetric distributions of the magnetic field with respect to the middle plane of the film (membrane). We will refer to these plasmons as symmetric and anti-symmetric film plasmons, respectively. This is similar to the terminology used in [20] for the symmetric and anti-symmetric gap plasmons. The dispersion relationships for the symmetric and anti-symmetric film plasmons, respectively, are given by the equations [28]:

$$\tanh\left(\frac{\alpha_2 f}{2}\right) = -\frac{\alpha_1 \varepsilon_2}{\alpha_2 \varepsilon_1}, \tag{1}$$

$$\tanh\left(\frac{\alpha_2 f}{2}\right) = -\frac{\alpha_2 \varepsilon_1}{\alpha_1 \varepsilon_2}, \tag{2}$$

where,

$$\alpha_1 = \sqrt{q^2 - k_0^2 \varepsilon_1}, \qquad \alpha_2 = \sqrt{q^2 - k_0^2 \varepsilon_2} \tag{3}$$

are the reciprocal penetration depths of the plasmon into the dielectric and metal, respectively, $q = Q_1 + iQ_2$ is the complex wave number of the plasmon (Q_2 determines dissipation of the plasmon), $k_0 = \omega/c$ is the wave number in vacuum, and f is the thickness of the film (membrane):

$$f = 2y \tan(\gamma/2), \tag{4}$$

Note that Eqs. (1) and (2) are also valid for the description of the coupled plasmons in a dielectric gap (with the permittivity ε_1 between two identical metals with the permittivities ε_2) [28]. However, in that case, Eq. (1) gives the dispersion of the anti-

symmetric gap plasmon, whereas Eq. (2) determines the dispersion of the symmetric gap plasmon [20].

In this paper, we assume that dissipation of the plasmons is weak, i.e. $e_2 << |e_1|$ and $Q_2 << Q_1$. The opposite case is not interesting, because if dissipation is strong, the plasmon will not be able to propagate noticeable distances in the structure and experience effective nano-focusing.

As the anti-symmetric or symmetric film plasmon propagates towards the tip of the wedge, it experiences changing thickness of the wedge (film). This means that the effective dielectric permittivity of the structure $\varepsilon_{eff} = (q/k_0)^2$ also changes, because the wave number of the plasmon q depends on changing thickness of the wedge (film). Propagation of the film plasmon can be considered in the geometrical optics approximation (GOA) (or, using the terminology of quantum mechanics, in the WKB approximation), if variations of the wave vector of the plasmon are small within distances of the order of one wavelength in the structure [7,20,29]:

$$|d(Q_{1y}^{-1})/dy| << 1, \qquad (5)$$

where Q_{1y} is the y-component of the real part of the wave vector **q** of the plasmon in the structure (Fig. 1b). In this case, the wedge is actually a metal film with slowly changing thickness. Therefore, at all points where condition (5) is satisfied, the parameters of the film plasmon (including its dispersion, dissipation and field structure) can be approximately determined by considering this plasmon in a uniform film of thickness that is equal to the local thickness of the wedge at the considered point. In this case, propagation of the plasmon in the wedge can be represented by a plasmon ray, i.e., a

curve such that the wave vector of the film plasmon is parallel to the curve at every point. An example of such a ray for the anti-symmetric film plasmon is shown in Fig. 1b.

For weak dissipation, numerical solution of the dispersion relationships (1), (2) gives real parts Q_1 of the plasmon wave numbers as functions of local thickness of the triangular silver wedge for anti-symmetric (Fig. 2a) and symmetric (Fig. 2b) film plasmons. The dependencies in Figs. 2a,b are presented for different permittivities of the surrounding dielectric and different wavelengths resulting in different real parts of the metal permittivities.

In particular, it can be seen that the wave numbers of the anti-symmetric film plasmons tend to infinity with decreasing thickness of the wedge (film) to zero, i.e., with decreasing distance to the tip of the wedge. On the contrary, the wave numbers of the symmetric plasmons are relatively unaffected by decreasing thickness of the wedge (Fig. 2b). In fact, the wave numbers of the symmetric plasmons reduce to the wave numbers of the bulk waves in the surrounding dielectric, as wedge thickness tends to zero near the tip. Thus the variation of the wave number of a symmetric film plasmon may only occur between the wave number of the plasmon on an isolated metal-dielectric interface and the wave number of the bulk wave in the surrounding dielectric (Fig. 2b). This is also the reason for decreasing the effect of wedge thickness on the wave numbers of the symmetric plasmons, when the ratio $|e_1|/\varepsilon_1$ is increased. In this case, the wave number of the surface plasmon on the isolated metal-dielectric interface becomes closer to the wave number of the bulk wave in the surrounding dielectric, resulting in decreasing range of possible wave numbers of the symmetric film plasmon (compare curves 1 – 4 in Fig. 2b).

For comparison, wave numbers of the symmetric and anti-symmetric gap plasmons propagating in a sufficiently sharp V-groove in silver are shown as functions of

local groove width in Figs. 3a,b for the same material parameters as in Figs. 2a,b (Fig. 3a is reproduced from [20]). In particular, it can be seen that the dependencies of the wave numbers of anti-symmetric plasmons in sharp metal wedges are very similar to those for the symmetric gap plasmons in sharp V-grooves (compare Figs. 2a and 3a). This suggests significant similarities in nano-focusing of these plasmons by wedges and grooves. Indeed, both these figures demonstrate that anti-symmetric plasmons in sharp triangular wedges and symmetric plasmons in V-grooves (see also [20]) experience adiabatic stopping near the tip. This will occur for all angles of incidence $\theta_0 < \pi/2$ (Fig. 1b). As the anti-symmetric film plasmon propagates towards the tip of the wedge, the *y*-component Q_{1y} of the real part $\mathbf{Q}_1$ of its wave vector $\mathbf{q}$ increases to infinity, while the *x*-component remains constant (due to Snell's law and uniformity of the wedge along the *x*-axis – Fig. 1a). Therefore, irrespective of the initial incidence angle θ_0 (as long as $\theta_0 < \pi/2$), the wave vector of the anti-symmetric wedge plasmon near the tip is perpendicular to the *x*-axis, which makes the plasmon ray turn perpendicular to the tip of the wedge (Fig. 1b). Note however, that these conclusions are correct only if the applicability condition (5) for GOA is satisfied for all values of *y*. In this case, no reflection occurs from the tip of the wedge; the plasmon propagating towards the tip adiabatically slows down, and eventually dissipates in the metal. This occurs in a very similar fashion as for symmetric plasmons in sufficiently sharp V-grooves [20].

Near the tip, the local thickness of the wedge tends to zero. In this case, if the condition

$$f\mathrm{Re}(\alpha_2) << 1, \qquad (6)$$

then Eq. (2) (for the anti-symmetric film plasmon) gives:

$$Q_1 \approx -2\varepsilon_1/(e_1 f). \quad (7)$$

Substituting Eq. (7) back into condition (6), it can be seen that at $f \to 0$ (i.e., near the tip of the wedge), condition (6) can be satisfied only if $\varepsilon_1/|e_1| << 1$, which is usually the case for good metals. This is also the applicability condition for the asymptotic behavior of the wave number of the anti-symmetric film plasmon (Eq. (7)) near the tip of the wedge.

On the contrary, the dependencies of the wave numbers of the symmetric film plasmons and anti-symmetric gap plasmons (Figs. 2b and 3b) are quite different. As indicated above, near the tip of the wedge (i.e., where $f \to 0$) the wave number of the symmetric film plasmon tends to the wave number of the bulk wave in the surrounding dielectric (Fig. 2b). In this case, the penetration depth of the symmetric film plasmon into the surrounding dielectric tends to infinity, and the film plasmon turns into a non-localized bulk wave in the dielectric. Therefore, symmetric film plasmons cannot be used for nano-focusing in sharp wedges.

The wave number of the anti-symmetric gap plasmon becomes zero at the cut-off gap width (Fig. 3b), below which the gap plasmon does not exist as a propagating wave. This plasmon can still be localized beyond the diffraction limit with the region of localization limited by the cut-off gap width. For example, this cut-off width for curve 1 in Fig. 3b is ~ 200 nm. However, anti-symmetric gap plasmons cannot experience unlimited (in the absence of dissipation) adiabatic nano-focusing like symmetric gap plasmons and anti-symmetric film plasmons.

The above analysis is valid if the applicability condition for GOA (Eq. (5)) is satisfied. Fig. 4 presents the typical dependencies of the applicability term in the left-hand

side of Eq. (5) on the *y*-coordinate (distance from the tip) for the anti-symmetric film plasmon (Fig. 4a), symmetric film plasmon (Fig. 4b), and anti-symmetric gap plasmon (Fig. 4c). The structural and material parameters are as indicated in the figure caption. The similar dependencies for the symmetric gap plasmon are presented in [20]. GOA is only applicable when the presented curves in Figs. 4a-c are noticeably below 1. For example, for the structures corresponding to curves 3 – 5 in Fig. 4a (i.e. for the anti-symmetric film plasmon), GOA is applicable at all distances from the tip of the wedge, because these curves are noticeably below 1 at all values of *y*. However, for the wedges corresponding to curves 1-2, GOA is only applicable for distances above the tip $y \gtrsim 0.2$ μm. This is again similar to symmetric gap plasmons in sharp V-grooves [20].

GOA is very well applicable for the analysis of symmetric film plasmons in the considered sharp wedges at all distances from the tip, which follows from Fig. 4b. Near the tip, the wave numbers of these plasmons tend to the wave numbers of bulk waves in the surrounding dielectric (Fig. 2b). Therefore, at small distances from the tip, variations of these wave numbers within distances of the order of one wavelength become negligible, and the applicability term tends to zero (Fig. 4b). However, it is important to note that these symmetric film plasmons are useless from the view-point of nano-focusing, as they are very weakly localized near the tip of the wedge.

On the contrary, for the anti-symmetric gap plasmon in a sharp V-groove, the applicability term turns to infinity at the cut-off thickness of the gap. This is also expected, because at this thickness the wave number of the anti-symmetric gap plasmon turns to zero (see Fig. 3b and its discussion). The corresponding wavelength becomes infinite, and even for arbitrarily sharp grooves variation of the structural parameters (e.g.,

width of the groove) within one wavelength becomes infinitely large, resulting in the applicability term in the left-hand side of Eq. (5) also turning to infinity (Fig. 4c).

Note also that, as follows from Figs. 4a-c, decreasing magnitude of the real part of the metal permittivity and increasing permittivity of the dielectric in contact result in improving applicability of GOA for anti-symmetric film plasmons (Fig. 4a), symmetric and anti-symmetric gap plasmons (see Fig. 4c and [20]), but has the opposite effect for the symmetric film plasmons (Fig. 4b). This is because the symmetric film plasmons experience larger range of variations of their wave numbers, if $|e_1|$ is decreased and ε_1 is increased (see above). This results in larger variations of the wave parameters within one wavelength in the structure, leading to worsening of the GOA applicability. On the other hand, for example, for anti-symmetric film plasmons, reducing $|e_1|$ and increasing ε_1 results in decreasing penetration depth of the plasmons into the metal wedge. This leads to decreasing coupling between the plasmons across the wedge, and thus decreasing the effect of changing wedge thickness. Therefore, the applicability conditions for GOA are easier to satisfy. It is also obvious that decreasing wedge (gap) angle also result in improving applicability of GOA for all structures.

Furthermore, for all the types of coupled plasmons in wedges/grooves, GOA is always applicable at relatively large distances from the tip (large values of *y*). This is because the surface plasmons forming the coupled film or gap plasmons are not strongly coupled across the wedge/gap of sufficiently large thickness/width. Therefore, variations of this thickness/width does not have a significant effect on the plasmons, resulting in good applicability of GOA. Thus, applicability of GOA is generally improved at sufficiently large distances from the tip – Figs. 4a-c (see also [20]). This is a significantly distinguishing feature between GOA and the previously developed approximate method

of analysis of plasmons in sharp wedges/grooves, that is normally applicable only in the immediate proximity of the tip [25].

As discussed above, near the tip of the wedge, the wave vector of the anti-symmetric plasmon is always perpendicular to the tip (Fig. 1b). This is because Q_{1y} becomes very large (see Eq. (7)) when $f \to 0$, i.e. near the tip. In this case, $Q_{1y} \approx Q_1$. Using this relationship together with Eqs. (4) and (7), condition (5) can be reduced as

$$\left|\frac{d(Q_{1y}^{-1})}{dy}\right| \approx -\frac{\gamma e_1}{2\varepsilon_1} << 1, \qquad (8)$$

or

$$\gamma << \gamma_{c2} = -2\varepsilon_1/e_1, \qquad (9)$$

where γ_{c2} is the critical angle of the wedge, such that GOA is applicable only for wedge angles that are noticeably smaller than γ_{c2} (the reason for using the index 2 will be clear below). For a silver wedge in vacuum at λ_{vac} = 0.6328 μm (He-Ne laser), we have $e_1 = -16.22$ [30,31], and $\gamma_{c2} \approx 7^o$. For example, curve 3 in Fig. 4a is lies significantly below 1, as this curve corresponds to the silver wedge with $\gamma = 2^o < \gamma_{c2}$.

Eqs. (8) and (9) are again similar to those obtained for symmetric plasmons in sharp V-grooves [20], as well as the dependencies in Fig. 4a (that are similar to the same applicability curves obtained for symmetric gap plasmons in [20]). In the same way as for the symmetric gap plasmons [20], all the curves in Fig. 4a tend to plateaus at small distances from the tip. These plateaus are determined by the ratio in the left-hand side of Eq. (8), which does not depend on local wedge thickness *f*.

If the condition $\gamma << \gamma_{c2}$ is not satisfied, then the anti-symmetric film plasmon will experience significant reflections in the wedge as it propagates towards the tip. Physically, these reflections will occur at every point on the ray where the applicability condition for GOA is not satisfied. Decreasing real part of the metal permittivity e_1 and increasing permittivity ε_1 of the surrounding dielectric medium result in increasing critical angle γ_{c2}, and the GOA applicability condition for the anti-symmetric film plasmon becomes less restrictive (Fig. 4a).

3. Plasmon Rays

Plasmon rays are determined by the angle θ between the plasmon wave-vector and the *y*-axis (Figure 1b). The algorithm for the determination and plotting of plasmon rays for the anti-symmetric film plasmons is the same as for the symmetric gap plasmons [20]. It can briefly be outlined as follows: if we know the position of some point with the coordinates (x,y) on the ray, then the position of the next point with the coordinated $(x + dx, y + dy)$ on the same ray is determined by the angle θ at the point (x,y) and the value of dy. Thus, the plasmon ray can be determined if we know the position of some initial point through which the plasmon ray propagates (for more detailed discussion of the algorithm see [20]). Suppose that this point is chosen on the y-axis. Then the typical plasmon rays for different incidence angles θ_0 and different wedge angles are presented in Fig. 5a.

For comparison, plasmon rays in the inversed structure, i.e., a metal groove rather than a wedge, are presented in Fig. 5b for the symmetric gap plasmons [20]. The angles of the silver wedge in vacuum (Fig. 5a), and vacuum groove in a silver substrate (Fig. 5b) are the same for the corresponding sets of curves. As can be seen, the rays of the anti-symmetric film plasmon in a wedge and symmetric gap plasmon in a groove are orthogonal to the *x*-axis at $y = 0$. However, in the wedge, the plasmon rays start to bend

when they come significantly closer to the tip than in grooves, and thus the anti-symmetric film plasmon reaches the tip of the wedge at a larger value of x than the corresponding symmetric gap plasmon (compare Figs. 5a,b). This is because film plasmons are formed by surface plasmons coupled across the metal wedge, while the gap plasmons are formed by surface plasmons coupled across the vacuum gap. Plasmon penetration depth into the metal is smaller than in vacuum, which means that coupling in the film plasmon weakens faster with increasing thickness of the wedge than coupling in the gap plasmon with increasing width of the gap. As a result, the wave number in the anti-symmetric film plasmon decreases faster with increasing thickness of the wedge, and coupling across the wedge has a significant effect on the wave number only in the region significantly closer to the tip (Fig. 5a) than for symmetric gap plasmons (Fig. 5b).

4. Nano-focusing of plasmons

As the anti-symmetric film plasmon approaches the tip of the wedge, it adiabatically slows down, i.e., its phase and group velocities turn to zero (similar to the symmetric gap plasmon in a metallic gap [20]). This means that the anti-symmetric plasmon experiences infinite (in the approximation of continuous electrodynamics) nano-focusing as it propagates towards the tip of the wedge.

The amplitude of the anti-symmetric film plasmon as it propagates towards the tip of the wedge is determined by the same procedure that has been developed for nano-focusing of the symmetric plasmon in a sharp V-groove [20]. Let us first assume that dissipation in the metal is zero, i.e., $\varepsilon_2 = e_1$ is real and negative. Because the structure is uniform along the x-axis (along the tip of the wedge), the energy conservation gives [20]:

$$S_0 \cos\theta_0 = S\cos\theta, \qquad (10)$$

where S_0 is the energy flux in the film plasmon at large distance from the tip of the wedge where the anti-symmetric film plasmon is represented by two uncoupled surface plasmons (Fig. 1b), and S and θ are the energy flux and angle of propagation of the plasmon at an arbitrary point on the plasmon ray. Note again that Eq. (10) is valid only in the assumption of zero dissipation in the metal.

The energy flux S in the anti-symmetric film plasmon at an arbitrary wedge thickness f is given by the Poynting vector averaged over the period of the wave $2\pi/\omega$ and integrated over the z-coordinate from $-\infty$ to $+\infty$:

$$S = \frac{c^2 Q_1}{16\pi\omega}\left|H_{20}\right|^2\left[\frac{2}{\varepsilon_1\alpha_{10}} + \frac{\sinh(\alpha_{20} f)}{e_1\alpha_{20}\sinh^2(\alpha_{20} f/2)} - \frac{f}{e_1\sinh^2(\alpha_{20} f/2)}\right], \quad (11)$$

where H_{20} is the amplitude of the magnetic field at either of the metal interfaces at the considered distance from the tip, and

$$\alpha_{10} = \sqrt{Q_1^2 - k_0^2\varepsilon_1}\,, \quad \alpha_{20} = \sqrt{Q_1^2 - k_0^2 e_1}\,. \quad (12)$$

Thus, in order to obtain the amplitude of the incident anti-symmetric plasmon as a function of distance from the tip of the wedge in the absence of dissipation, we use the following procedure [20]. Determine (numerically) Q_1 from Eq. (2) for different values of f (Fig. 2a), which automatically gives the dependence of Q_1 on y – see Eq. (4). Use the Snell law

$$Q_{01}\sin\theta_0 = Q_1\sin\theta \quad (13)$$

(where Q_{01} is the real part of the wave number $q_0 = Q_{01} + iQ_{02}$ of the film plasmon at $y \to +\infty$) to determine the angle θ between the wave vector of the anti-symmetric plasmon and the y-axis. Calculate $S(y)$ from Eq. (11), and use Eq. (10) to determine the amplitude of

the plasmon $H_{20}(y)$, assuming that the amplitude of the incident plasmon at infinity H_{200} = 1 (recall that we consider the structure without dissipation).

Fig. 6 shows the typical y-dependencies of the amplitudes $H_{20}(y)$ of the anti-symmetric film plasmons at zero dissipation in the metal (e_2 = 0). Similar to the symmetric gap plasmons in sharp V-grooves [20], the anti-symmetric film plasmons also increase their amplitudes as they propagate towards the tip of the wedge (Fig. 6). However, this increase is not as strong as for the symmetric gap plasmons, and is only about ~ 1.5 – 2 times, compared to 4 – 12 times for the symmetric gap plasmons [20].

The dependencies in Fig. 6 are plotted starting from 30 nm distance from the tip of the wedge. This is because at this distance the typical thickness of the wedge becomes ~ 1 nm, and for smaller thicknesses the approximation of continuous electrodynamics is not applicable [32,33]. At the same time, as can be seen from Fig. 6, the maximal amplitudes of the film plasmons are achieved at distances of ~ 100 nm from the tip, where the developed theory is well applicable.

Increasing the permittivity of the surrounding dielectric results in decreasing maximal plasmon amplitude (compare curves 2 and 4, and curves 1 and 3 in Fig. 6a). However, increasing the magnitude of the metal permittivity results in increasing efficiency of nano-focusing in terms of the local field enhancement (curves 1 and 4 in Fig. 6a). This is very similar to what was predicted for the symmetric gap plasmon in a V-groove [20]. Therefore, to increase local field enhancement near the tip of the wedge, one should increase the ratio $|e_1|/\varepsilon_1$. However, applicability of GOA worsens with increasing ratio $|e_1|/\varepsilon_1$ (Section 2), and this may eventually lead to noticeable reflections from the tip of the wedge (similar to the grooves for which GOA is not applicable [20,34]).

Increasing θ_0 results in decreasing local field enhancement near the tip (Fig. 6b). This is related to the fact that increasing angle of incidence θ_0 results in decreasing *y*-component of the energy flux in the incident plasmon. If dissipation is zero, then according to energy conservation, this flux component should remain constant (in GOA) along the plasmon ray [20]. On the other hand, when $y \to 0$ the plasmon ray becomes normal to the tip of the wedge (see Figs. 1b, 5a). Therefore, near the tip, the energy flux in the plasmon is always perpendicular to the tip, i.e., parallel to the *y*-axis. This means that decreasing *y*-component of the incident energy flux (i.e., increasing θ_0) causes decreasing energy flux in the plasmon near the tip, i.e., decreasing its amplitude – compare curves 1, 3, 4 in Fig. 6b (see also [20]).

Similar to nano-focusing in V-grooves [20], decreasing wedge angle results in increasing distance from the tip of the wedge, at which the maximal local field enhancement is achieved (compare cures 2 and 3 in Fig. 6b). This is because in GOA and in the absence of dissipation, the plasmon amplitude is determined by the size of the localization region where the energy is concentrated due to nano-focusing, but not by distance that the plasmon should travel to reach this localization region. On the other hand, plasmon localization depends on local thickness of the wedge (localization increases with decreasing local thickness), and the same wedge thicknesses are achieved at larger distances if the angle γ is decreased.

Another similarity between nano-focusing in V-grooves [20] and sharp triangular wedges is that in both these cases the local enhancement of the field near the tip is finite, i.e., all the curves in Fig. 5 tend to plateaus when $y \to 0$. However, the actual values of the field enhancement, corresponding to the plateaus, are significantly smaller for the wedges compared to the grooves. The plateaus of the plasmon amplitude in the wedge (Fig. 6) can

be understood by considering Eq. (11) at $f \to 0$ (which is equivalent to $y \to 0$). In this case, Eq. (11) is reduced as

$$S \approx \frac{c^2}{8\pi\omega\varepsilon_1}|H_{20}|^2, \qquad (14)$$

which is independent of y. As a result, the corresponding amplitude of the plasmon is also y-independent – see the plateaus in Fig. 6. The differences in the plateau height for gap plasmons [20] and film plasmons (Fig. 6) are due to the fact that Eq. (14) contains ε_1 in the denominator, as opposed to $|e_1|$ for the gap plasmons [20]. Indeed, Eq. (10) suggests that near the tip $S_0\cos\theta_0 = S$ (because in this case $\theta = 0$) for both the wedge and groove – see also [20]. For example, for the wedge, substituting here Eqs. (14) and (11), and assuming that the initial point is sufficiently far from the tip, so that there is no coupling between the plasmons on the wedge sides ($\alpha_{20}f >> 1$), we obtain the amplitude at the tip of the wedge:

$$|H_{20}|^2 = Q_1\varepsilon_1[(e_1\alpha_{20})^{-1} + (\varepsilon_1\alpha_{10})^{-1}]|H_{200}|^2\cos\theta_0,$$

where H_{200} is the amplitude of the incident plasmon at $y \to +\infty$ (i.e., where $\alpha_{20}f >> 1$). Similar equation for the groove [20] gives

$$|H_{20}|^2 = Q_1|e_1|[(e_1\alpha_{20})^{-1} + (\varepsilon_1\alpha_{10})^{-1}]|H_{200}|^2\cos\theta_0.$$

From here, it is obvious that the amplitude of the adiabatically focused film plasmon at the tip of the wedge is $(|e_1|/\varepsilon_1)^{1/2}$ times smaller than that of the gap plasmon at the tip of the V-groove – compare Fig. 6 with Fig. 5 from [20].

It is important that enhancement of the local field near the tip of the wedge/gap is not the necessary condition for nano-focusing. Nano-focusing, i.e., localization of the

electromagnetic energy in a region that is much smaller than the wavelength, may occur if there is no field enhancement (see, for example, curve 4 in Fig. 6b). However, the additional effect of field enhancement may be useful in practical applications such as design of new optical sensors, near-field optical microscopy and spectroscopy, etc.

As has been shown in [20], dissipation in the metal may play a significant role in plasmon nano-focusing, especially for the local field enhancement. For arbitrary dissipation the metal permittivity $\varepsilon_2 = e_1 + ie_2$ ($e_2 > 0$) and the energy flux in the anti-symmetric film plasmon at a given film thickness f can be written as:

$$S = \frac{c^2}{8\pi\omega}\left|H_{20}\right|^2 \exp(-2x_p Q_2)\left[\frac{\mathrm{Re}(q/\varepsilon_1)}{\mathrm{Re}(\alpha_1)} + \frac{\mathrm{Re}(q/\varepsilon_2)}{\mathrm{Re}(\alpha_2)}\frac{\sinh[f\,\mathrm{Re}(\alpha_2)]}{2\left|\sinh(\alpha_2 f/2)\right|^2} - \right.$$

$$\left. - \frac{\mathrm{Re}(q/\varepsilon_2)}{\mathrm{Im}(\alpha_2)}\frac{\sin[f\,\mathrm{Im}(\alpha_2)]}{2\left|\sinh(\alpha_2 f/2)\right|^2}\right], \qquad (15)$$

where x_p is the coordinate in the direction of plasmon propagation. As mentioned in [20], the amplitude of the plasmon H_{20} cannot be chosen to equal 1 at $y = +\infty$, because in this case it would have been zero at any finite value of y. Therefore, we choose that $H_{20} = 1$ at some reference point on the plasmon ray, and the specific choice of this point will be discussed below.

In the case of weak dissipation, i.e., when $e_2 << |e_1|$ and $Q_2 << Q_1$, Eq. (2) gives for the anti-symmetric film plasmon:

$$Q_2 \approx \frac{\alpha_{10} e_2 k_o^{\,2}(\alpha_{10}^{\,2} e_1^{\,2} f - \alpha_{20}^{\,2}\varepsilon_1^{\,2} f + 2\alpha_{10} e_1\varepsilon_1)/2 + 2\alpha_{20}^{\,2}\varepsilon_1 e_2 \alpha_{10}^{\,2}}{Q_1[\,f\alpha_{10}^3 e_1^2 - f\alpha_{10}\alpha_{20}^2\varepsilon_1^2 - 2e_1\varepsilon_1(\alpha_{20}^2 - \alpha_{10}^2)]}, \qquad (16)$$

where Q_1 is determined numerically using Eq. (2) under the assumption that $e_2 = 0$.

The numerical procedure developed in [20] for the determination of the plasmon amplitude along a plasmon ray in the presence of dissipation can be directly applied for the analysis of nano-focusing of anti-symmetric film plasmons in sharp wedges. The resultant dependencies of the plasmon amplitudes on distance from the tip of the wedge are presented in Fig. 7 for silver wedges at different wavelengths.

It can be seen that at large distances from the tip of the wedge, the amplitude of the film plasmon propagating towards the tip decreases exponentially, goes through a minimum, and then strongly increases reaching a maximum. Further decrease of distance to the tip of the wedge results in a monotonous decrease of the plasmon amplitude (Figs. 7a,b). All the curves in Figs. 7a,b are normalized to the amplitude of the plasmon at the mentioned minimum. This means that the reference point with the amplitude $H_{20} = 1$ is always chosen at the minimum of the plasmon amplitude (Figs. 7a,b).

The exponential decrease of the plasmon amplitude at large distances from the wedge tip can be explained by weak coupling of the surface plasmons forming the anti-symmetric film plasmon at large thicknesses of the wedge. Because the coupling is weak, the predominant mechanism of changing plasmon amplitude is dissipation in the metal. When the plasmon comes closer to the tip, so that coupling across the wedge is significant (due to decreasing thickness of the wedge), the effect of nano-focusing increases (Fig. 6) and may overpower dissipation. As a result, the plasmon amplitude starts to increase. However, in the vicinity of the tip, the amplitude growth caused by nano-focusing ceases (see the plateaus in Fig. 6). As a result, if dissipation is sufficiently weak, the plasmon amplitude reaches a maximum at an optimal distance from the tip, and then monotonically decreases to zero when $y \to 0$ (Fig. 7). If dissipation is increased the amplitude maximum decreases (Fig. 7), and eventually disappears altogether (curve 5 in Fig. 7a).

Similar to the case with no dissipation (Fig. 6), Fig. 7b demonstrates that decreasing angle of incidence results in increasing maximal local field enhancement near the tip of the wedge. The explanation of this is similar to that presented for Fig. 6 with no dissipation. Increasing wedge angle also results in increasing local field enhancement (Fig. 7b). This is because increasing wedge angle causes more rapid variations of the wedge thickness. Therefore, in order to experience significant amplitude enhancement due to nano-focusing, the plasmon should travel smaller distance along the *y*-axis, which means smaller effect from dissipation. The distance from the tip, at which the maximum of the plasmon amplitude is reached, decreases with increasing wedge angle.

As discussed in [20], the choice of normalization of the plasmon amplitude, so that it is equal to 1 at the local minimum (Figs. 7a,b), is useful, because it immediately shows the maximal possible enhancement of the plasmon field during nano-focusing. This enhancement is then given by the local maximum of the plasmon amplitude (Figs. 7a,b). Therefore, up to ~ 2 times enhancement of the local field can be achieved in the considered wedge structures. For the experimental observation of this enhancement, the wedge should be cut to form a trapezium (Fig. 8). The distances from the tip, at which the wedge should be cut, must correspond to the distances from the tip, at which the local minimum and maximum of the plasmon amplitude are achieved (Fig. 7). Therefore, the height of the trapezium h_w (Fig. 8) should be equal to the distance between the local minimum and maximum of the corresponding dependence in Fig. 7.

For example, for curve 1 in Fig. 7b, the local minimum of the plasmon amplitude is achieved at $y \approx 2$ μm, whereas the local maximum is obtained at $y \approx 70$ nm. Therefore, the corresponding height of the trapezium should be $h_w \approx 1.930$ μm with the width of the bases $f_{entry} \approx 140$ nm and $f_{exit} \approx 5$ nm (Fig. 8). In this case, if the coupled film plasmon is

generated in the trapezium-like wedge, e.g., by means of the end-fire excitation (as shown in Fig. 8), then the maximal possible local field enhancement will be achieved at the exit base of the wedge of ~ 1.8 times for the material and structural parameters corresponding to curve 1 in Fig. 7b.

Note again that the considered analysis is valid only in the case of relatively weak dissipation of the anti-symmetric film plasmons, i.e., when $Q_2 << Q_1$. It can be shown that the typical ratio of Q_2/Q_1 for all the presented curves is below ~ 0.07, which suggests that the condition of weak dissipation is satisfied.

5. Wedge plasmons

It has been predicted theoretically (via finite-difference time-domain (FDTD) algorithm) and verified experimentally that a special type of strongly localized plasmon (wedge plasmon) can exist and be guided by a triangular metal wedge [26]. That is, the wedge acts as a new type of sub-wavelength waveguide [26]. This occurs if the wedge angle is smaller than the critical angle γ_{c1} (which in the case of the silver-vacuum structure and λ_{vac} = 0.6328 μm is $\gamma_{c1} \approx 102^o$ [26]). Wedge plasmons are strongly localized near the tip of the wedge and propagate infinite distance along this wedge, if there is no dissipation in the metal. Therefore they are structural eigenmodes of the metal wedge [26].

It has also been shown that V-grooves on a metal surface can also guide strongly localized plasmons that were called channel plasmon-polaritons (CPPs) [20, 35-40]. The analysis of CPP modes has mainly been conducted using the FDTD approaches [36-38]. In particular, it was shown that such modes can exist in a V-groove only if the groove

angle is smaller than the upper critical angle (similar to γ_{c1} for wedge plasmons [26]). Recently, GOA-based analysis has also demonstrated that in addition to the upper critical angle there also exists a lower critical angle of the groove, below which CPP modes cannot exist [20]. This is because below the lower critical angle, GOA is applicable to the plasmons in the groove (tapered gap), and these plasmons experience adiabatic nano-focusing. As a result, localization of CPP modes near the tip of the groove appears to be infinite, i.e., such modes do not exist [20]. Therefore, CPP modes can exist in V-grooves only within the range of groove angles between the upper and lower critical angles [20].

The demonstrated analogy between adiabatic nano-focusing of symmetric gap plasmons (forming CPP modes [20]) and anti-symmetric film plasmons suggests that we should probably be able to use GOA to derive additional existence conditions for strongly localized wedge plasmons.

Similar to [20], in order to find these conditions, we represent a wedge plasmon mode in a sufficiently sharp triangular metal wedge by means of an anti-symmetric film plasmon propagating in the metal wedge/film with slowly varying thickness. If condition (5) is satisfied, GOA is applicable for the analysis of such anti-symmetric film plasmon. The effective dielectric permittivity experienced by this film plasmon as it propagates in the wedge is defined as $\varepsilon_{eff} = [Q_1(y)c/\omega]^{1/2}$. It increases with decreasing distance to the tip of the wedge, due to increasing Q_1 (see Eq. (7) and Fig. 2a). Thus the wedge forms a kind of a waveguide for the anti-symmetric film plasmon with gradually changing permittivity ε_{eff}. A localized wedge plasmon mode could then be represented by an anti-symmetric film plasmon successively reflecting from the tip of the wedge and the turning point (simple caustic) – Fig. 9. The wave vector of the localized wedge plasmon mode is equal to the x-component of the wave vector of the anti-symmetric film plasmon $q_{wp} = Q_{1x}$.

Note that the main difference between this situation and the previously considered nano-focusing of the anti-symmetric film plasmon is that in the case of a wedge plasmon mode no incident film plasmon exists. The film plasmon representing the wedge plasmon mode is confined to a region close to the tip of the wedge and cannot leave this region, which makes wedge plasmon modes non-radiative structural eigenmodes [26]. This representation is very similar to the representation of a guided non-radiative mode of a dielectric slab by means of a bulk wave successively reflecting from the slab interfaces.

Only anti-symmetric film plasmons can be used for the representation of wedge plasmon modes. This is because the effective permittivity for the symmetric film plasmon (as well as its wave vector) decreases with decreasing distance from the tip of the wedge (Fig. 2b). As a result, no guiding effect near the tip can be achieved in this case.

The turning point y_t (simple caustic) is then determined by the condition $Q_1(y)\big|_{y=y_t} = q_{wp}$. In this case, the anti-symmetric film plasmon representing the wedge plasmon mode propagates parallel to the tip (Fig. 9).

However, using GOA for the determination of wave numbers of the wedge plasmons modes is not possible, similar to CPP modes in V-grooves [20]. This is because the Bohr-Sommerfeld quantization condition [20, 41, 42] that should determine the wave numbers of the wedge plasmon modes diverges at the tip of the wedge (as it did at the tip of the V-groove for symmetric gap plasmons [20]).

Physically, this is related to the fact that if GOA is applicable near the tip of the wedge (see conditions (5), (8) and (9)), then the anti-symmetric film plasmon propagating towards the tip at any possible angle θ will travel an infinite optical path until it reaches the tip. As indicated above, such plasmons cannot be reflected back from the tip even if

dissipation is ignored. The plasmon asymptotically stops at the tip and will thus have infinite localization. Therefore, the localization of the corresponding wedge plasmon mode near the tip of the wedge will also be infinite, $q_{wp} = +\infty$, and this corresponds to zero wavelength and velocity. In other words, the wedge plasmon mode does not exist.

Therefore, wedge plasmon modes do not exist in a wedge if GOA is applicable. On the contrary, if GOA is not applicable near the tip of the triangular metal wedge, then the divergence of the Bohr-Sommerfeld quantization condition does not have a physical meaning [20]. The anti-symmetric film plasmon representing a wedge plasmon mode is efficiently reflected as it propagates towards the tip of the wedge, and this is what is required for the representation of the wedge plasmon by the reflecting anti-symmetric film plasmon (Fig. 9).

Despite the fact impossibility of using GOA for the determination of wave numbers of wedge plasmon modes, the above consideration leads to important conclusions about the existence conditions of wedge plasmons. These plasmons can only exist if GOA is not applicable near the tip of the groove – this is where significant reflections of the film plasmon may occur. Thus, according to the applicability condition of GOA near the tip (Eqs. (8) and (9)), we can write the existence condition for wedge plasmon modes in a triangular metal wedge as follows:

$$\gamma \gtrsim \gamma_{c2}. \qquad (17)$$

This condition is thus opposite to inequality (9). It determines the lower critical angle γ_{c2} below which wedge plasmon modes do not exist in a triangular metal wedge. Thus, wedge plasmons exist only within the range of angles:

$$\gamma_{c2} \lesssim \gamma < \gamma_{c1}, \qquad (18)$$

where γ_{c1} was determined numerically in [26] as the upper critical angle above which wedge plasmons do not exist because they become coupled to surface plasmons on the sides of the wedge [26]. Now it is clear why we used the index "2" for the critical angle γ_{c2} (see also Eq. (9)). There are two critical angles determining the existence condition of wedge plasmon modes in a triangular metal wedge. For example, for a silver wedge in vacuum at the vacuum wavelength $\lambda_{vac} = 0.6328$ μm, we have $\gamma_{c1} \approx 102^o$ [26], and $\gamma_{c2} \approx 7^o$ (see above).

6. Conclusions

Using the geometrical optics approximation and the approximation of continuous electrodynamics, a possibility of effective nano-focusing of anti-symmetric film plasmons in sharp triangular metal wedges has been demonstrated. In particular, it was shown that under the mentioned approximations, these plasmons asymptotically stop at the tip of the wedge with both their phase and group velocities tending to zero, and the wave vector to infinity. As a result, an anti-symmetric film plasmon incident onto the tip of the wedge at an arbitrary angle does not experience reflection from the tip, but rather propagates an infinite optical path towards the tip, and eventually dissipates in the metal.

The considered adiabatic regime of nano-focusing of plasmons in a metal wedge may occur only if the wedge angle is smaller than the critical angle that is determined by the dielectric permittivities of the metal wedge and the surrounding dielectric medium. Noticeable local field enhancement (~ 2 times) has been predicted near the tip of the wedge, though this enhancement is about 5 times weaker for the metal wedge than for the metallic V-groove [20]. The effect of dissipation on plasmon nano-focusing by means of a

metallic V-groove was analyzed in detail. In particular, optimisation of the geometrical and material parameters of the wedge structure for achieving maximal possible local field enhancement was carried out. The effect of angle of incidence and wavelength of the electromagnetic radiation on nano-focusing and local field enhancement in metal wedges was investigated theoretically. Applicability conditions for the obtained results and the adiabatic approximation were discussed.

It was demonstrated that it is not possible to use GOA for the determination of wave numbers of the strongly localized wedge plasmon modes guided by a triangular metal wedge, because of the divergence of the Bohr-Sommerfeld quantization condition near the tip of the wedge. However, the conducted analysis based on GOA has led to the determination of the lower critical angle of the wedge, below which wedge plasmon modes do not exist. Is was shown that wedge plasmon modes can only exist in the range of wedge angles between the lower critical angle ($\sim 7^o$ for a silver wedge in vacuum) and the previously determined upper critical angle ($\approx 102^o$ for silver wedge in vacuum [26]). Thus the conditions for adiabatic nano-focusing in sharp metal wedges are opposite to the conditions of existence of strongly localized wedge plasmon modes [26].

If conditions for GOA are not satisfied, then the theory developed in this paper fails and numerical methods of analysis (e.g., based on the FDTD algorithm) will be required. These numerical methods and the analysis of non-adiabatic nano-focusing of plasmons in tapered gaps and wedges have been developed in [34]. In particular, it has been shown that in the non-adiabatic regime of nano-focusing reflective energy losses in the plasmon as it propagates towards the tip may be noticeable and should be taken into account. These losses are added to the dissipative losses, resulting in a reduction of the local field enhancement near the tip [34].

The obtained results may be important for efficient energy coupling into nano-optical circuits, development of new optical sensors and measurement techniques, near-field microscopy and spectroscopy, design of new sub-wavelength plasmonic waveguides and interconnectors, etc.

References

1. A. V. Zayats, I. Smolyaninov: J. Opt. A: Pure Appl. Opt. 5, S16 (2003).
2. D. W. Pohl, W. Denk, M. Lanz: Appl. Phys. Lett. 44, 651 (1984).
3. L. Novotny, C. Hafner: Phys Rev. E 50, 4094 (1994).
4. A. Bouhelier, J. Renger, M. R. Beversluis, L. Novotny: J. Microsc. 210, 220 (2003).
5. F. Keilmann: J. Microsc. 194, 567 (1999).
6. H. G. Frey, F. Keilmann, A. Kriele, R. Guckenberger: Appl Phys. Lett. 81, 5030 (2002).
7. M. I. Stockman: Phys. Rev. Lett. 93, 137404, (2004).
8. S. Kawata: Topics in Applied Physics: Near-field Optics and surface plasmon-polaritons, vol. 81(Springer-Verlag, Berlin, 2001).
9. A. Naber, D. Molenda, U. C. Fischer, H.-J. Maas, C. Hoppener, N. Lu, and H. Fuchs: Phys. Rev. Lett. 89, 210801 (2002).
10. A.J. Babadjanyan, N.L. Margaryan, Kh.V. Nerkararyan: Journal of Appl. Phys. 87, 8 (2000).
11. Kh. V. Nerkararyan, T. Abrahamyan, E. Janunts, R. Khachatryan, S. Harutyunyan: Phys. Lett. A 350, 147 (2006).
12. L. Novotny, D.W. Pohl, B. Hecht: Ultramicroscopy 61, 1 (1995).
13. D. Mehtani, N.Lee, R.D. Hartschuh, A. Kisliuk, M.D. Foster, A.P. Sokolov, F.Cajko, I. Tsukerman: J. Opt. A. : Pure Appl. Opt. 8, S183 (2006).
14. N. Anderson, A. Bouhelier, L. Novotny: J. Opt. A: Pure Appl. Opt. 8, S227 (2006).
15. K. Kneipp, Y. Wang, H. Kneipp, L. T. Perelman, I. Itzkan, R. R. Dasari, M. S. Feld: Phys. Rev. Lett. 78, 1667 (1997).
16. B. Pettinger, B. Ren, G. Picardi, R. Schuster, G. Ertl: Phys. Rev. Lett. 92, 096101 (2004).

17. T. Ichimura, N. Hayazawa, M. Hashimoto, Y. Inouye, S. Kawata: Phys. Rev. Lett. 92, 220801 (2004).
18. S. M. Nie, S. R. Emory: Science 275, 1102 (1997).
19. R. Hillenbrand, T. Taubner, F. Kellmann: Nature 418, 159 (2002).
20. D.K. Gramotnev: J. Appl. Phys. 98, 104302 (2005).
21. D. Molenda, G. Colas des Francs, U.C. Fischer, N. Rau, A. Naber: Opt. Exp. 13, 10688 (2005).
22. G. Colas des Francs, D. Molenda, U.C. Fischer, A. Naber: Phys. Rev. B 72, 165111 (2005). .
23. S. Kawata, M. Ohtsu, M.Irie: Nano-optics (Springer, Berlin; New York, 2002).
24. E.Betzig, J.K. Trautman: Science 257, 189 (1992).
25. Kh.V. Nerkararyan: Phys. Lett. A 237**,** 103 (1997).
26. D.F.P.Pile, T.Ogawa, D.K.Gramotnev, T.Okamoto, M.Haraguchi, M.Fukui, S.Matsuo: Appl. Phys. Lett. 87, 061106 (2005).
27. H. Raether: Surface Plasmons (Springer-Verlag, Berlin, 1988).
28. J.J. Burke, G.I. Stegeman, T. Tamir: Phys. Rev B 33, 5186 (1986).
29. Yu. A. Kravtsov, Yu. I. Orlov: Geomentrical Optics of Inhomogeneous Media (Springer-Verlag, Berlin, 1990).
30. E. D. Palik: Handbook of Optical Constants of Solids (Academic, New York, 1985).
31. D.C.Fowers: Biosens. Bioelectron. 11, 677 (1996); D. Fowers: *Masters Thesis*, University of Utah (1994).
32. A. Liebsch: Phys. Rev. Lett. 54, 67 (1985).
33. I. A. Larkin, M. I. Stockman, M. Achermann, V. I. Klimov: Phys. Rev B 69, 121403(R) (2004).

34. D. F. P. Pile, D. K. Gramotnev, “Adiabatic and non-adiabatic nano-focusing of plasmons by tapered gap plasmon waveguides”: Appl. Phys. Lett. (submitted, February 2006).
35. I. V. Novikov, A. A. Maradudin: Phys. Rev. B66, 035403 (2002).
36. D. K. Gramotnev, D. F. P. Pile: Appl. Phys. Lett. 85, 6323 (2004).
37. D.F.P.Pile, D.K.Gramotnev: Opt. Lett. 30, 1186-1188 (2005).
38. D.F.P.Pile, D.K.Gramotnev: Appl. Phys. Lett. 86, 161101 (2005).
39. S.I. Bozhevolnyi, V.S. Volkov, E. Devaux, T.W. Ebbesen: Phys. Rev. Lett. 95, 046802 (2005).
40. S.I. Bozhevolnyi, V.S. Volkov, E. Devaux, T.W. Ebbesen: Nature 440, 508 (2006)
41. V. V. Krylov: Sov. Phys. Tech. Phys. 35(2), 137 (1990).
42. V. V. Krylov: Sov. Phys. Acoust. 36(2), 176 (1989).

Figure and Table Captions

Fig. 1. (a) An infinite triangular metal wedge with the angle γ and the permittivity ε_2, surrounded by a dielectric with the permittivity ε_1. (b) A ray representing the direction of propagation of an anti-symmetric film plasmon in the wedge in the geometrical optics approximation. θ_0 is the angle of propagation of the film plasmon at large distances from the tip of the wedge, where the coupling between the two surface plasmons representing the film plasmon is negligible.

Fig. 2. The dependencies of the real part of the wave number Q_1 of the anti-symmetric (a) and symmetric (b) film plasmon on wedge thickness f for the following material parameters: (1) $e_1 = -6.5$, $\varepsilon_1 = 1$, vacuum wavelength $\lambda_{vac} = 0.4592$ μm, (2) $e_1 = -16$, $\varepsilon_1 = 1$, $\lambda_{vac} = 0.6328$ μm, (3) $e_1 = -58.8$, $\varepsilon_1 = 2.5$, $\lambda_{vac} = 1.127$ μm, (4) $e_1 = -58.8$, $\varepsilon_1 = 1$, $\lambda_{vac} = 1.127$ μm. The real parts of the metal permittivities correspond to silver at the indicated wavelengths [30,31].

Fig. 3. The dependencies of the real part of the wave number Q_1 of the symmetric (a) and anti-symmetric (b) gap plasmon on gap width for the same material parameters as in Fig. 2: (1) $e_1 = -6.5$, $\varepsilon_1 = 1$, vacuum wavelength $\lambda_{vac} = 0.4592$ μm, (2) $e_1 = -16$, $\varepsilon_1 = 1$, $\lambda_{vac} = 0.6328$ μm, (3) $e_1 = -58.8$, $\varepsilon_1 = 2.5$, $\lambda_{vac} = 1.127$ μm, (4) $e_1 = -58.8$, $\varepsilon_1 = 1$, $\lambda_{vac} = 1.127$ μm. For this figure, ε_1 is the permittivity of the dielectric inside the gap, and e_1 is the real part of the permittivity of silver surrounding the gap (Fig. 3a is reproduced from Fig. 2a in [20]).

Fig. 4. The typical dependencies of the term in the left-hand side of inequality (5) for the anti-symmetric film plasmon (a), symmetric film plasmon (b), and anti-symmetric gap plasmon on distance from the tip (c). The angle of the wedge/gap is 2^o. (1) $e_1 = -96.6$, $\varepsilon_1 = 2.5$, $\lambda_{vac} = 1.631$ μm, (2) $e_1 = -58.8$, $\varepsilon_1 = 2.5$, $\lambda_{vac} = 1.127$ μm, (3) $e_1 = -16$, $\varepsilon_1 = 1$, $\lambda_{vac} = 0.6328$ μm, (4) $e_1 = -58.8$, $\varepsilon_1 = 5$, $\lambda_{vac} = 1.127$ μm, (5) $e_1 = -16$, $\varepsilon_1 = 2.5$, $\lambda_{vac} = 0.6328$ μm. Curve 3 in (a) also approximately corresponds to the other structure with $e_1 = -58.8$, $\varepsilon_1 = 2.5$, $\lambda_{vac} = 1.127$ μm, and $\beta = 1^o$. The real parts of the metal permittivities correspond to silver at the indicated wavelengths [30,31].

Fig. 5. Examples of plasmon rays for the anti-symmetric film plasmon in a triangular wedge (a), and symmetric gap plasmon in a V-groove (b). In both the cases, the metal is silver and dielectric is vacuum with $\varepsilon_1 = 1$ and $e_1 = -16$ [30,31] at the vacuum wavelength $\lambda_{vac} = 0.6328$ μm; the wedge/groove angles are: (1) 1^o, and (2) 2^o. Dashed curves: $\theta_0 = 75^o$, solid curves: $\theta_0 = 45^o$, and dotted curves: $\theta_0 = 25^o$. The initial y-coordinates for all the rays correspond to the ≈ 118 nm thickness/width of the wedge/groove.

Fig. 6. a) Normalized amplitudes of the magnetic field in the metal $H_{20}(y)/H_{200}$ ($H_{200} \equiv H_{20}(\infty)$) versus y for the anti-symmetric film plasmons incident onto the tip of the metal wedge with the angle $\gamma = 2^o$. There is no dissipation in the metal ($e_2 = 0$), the angle of incidence $\theta_0 = 0$, and the permittivities and the wavelengths are as follows: (1) $e_1 = -58.8$, $\varepsilon_1 = 2.5$, $\lambda_{vac} = 1.127$ μm, (2) $e_1 = -16$, $\varepsilon_1 = 1$, $\lambda_{vac} = 0.6328$ μm, (3) $e_1 = -58.8$, $\varepsilon_1 = 5$, $\lambda_{vac} = 1.127$ μm, (4) $e_1 = -16$, $\varepsilon_1 = 2.5$, $\lambda_{vac} = 0.6328$ μm. b) The dependencies $H_{20}(y)/H_{200}$ for the anti-symmetric film plasmons at $e_1 = -16$, $\varepsilon_1 = 1$, $\lambda_{vac} = 0.6328$ μm, and different values of θ_0 and γ: (1), $\theta_0 = 0$, $\gamma = 4^o$, (2) $\theta_0 = 45^o$, $\gamma = 1^o$, (3) $\theta_0 = 45^o$, $\gamma = 4^o$, (4) $\theta_0 = 75^o$, $\gamma = 4^o$. The metal permittivities correspond to the real parts of the permittivities of silver at the indicated wavelengths [30,31].

Fig. 7. The typical y-dependencies of the normalized amplitudes of the magnetic field $H_{20}(y)/H_{20min}$ in the anti-symmetric film plasmon (H_{20min} is the amplitude of the plasmon at the local minimum of the amplitude) incident onto the tip of the wedge in the presence of dissipation. (a) $\theta_0 = 0$, $\beta = 2^o$, and the other parameters are as follows: 1) $\lambda_{vac} = 1.127$ μm, $\varepsilon_2 = -58.8 + i$ (does not correspond to a particular metal), $\varepsilon_1 = 2.5$; 2) $\lambda_{vac} = 1.127$ μm, $\varepsilon_2 = -58.8 + 3.85i$ (silver), $\varepsilon_1 = 2.5$; 3) $\lambda_{vac} = 0.6328$ μm, $\varepsilon_2 = -16 + 0.52i$ (silver), $\varepsilon_1 = 1$; 4) $\lambda_{vac} = 0.6328$ μm, $\varepsilon_2 = -16 + i$ (silver), $\varepsilon_1 = 1$; 5) $\lambda_{vac} = 0.6328$ μm, $\varepsilon_2 = -16 + i$ (silver), $\varepsilon_1 = 2.5$. (b) $\varepsilon_2 = -16 + 0.52i$, $\varepsilon_1 = 1$, $\lambda_{vac} = 0.6328$ μm, and the angles: 1) $\theta_0 = 0$, $\gamma = 4^o$, 2) $\theta_0 = 0$, $\gamma = 2^o$, 3) $\theta_0 = 45^o$, $\gamma = 4^o$, 4) $\theta_0 = 45^o$, $\gamma = 2^o$, 5) $\theta_0 = 0$, $\gamma = 1^o$[30,31].

Fig. 8. The trapezium wedge of the optimal height h_w for maximal local field enhancement at the exit base of the trapezium. The anti-symmetric film plasmon is generated in the trapezium wedge by means of the end-fire excitation by an incident bulk wave focused onto the entry (larger) base of the trapezium of width f_{exit}. The maximal local field enhancement is thus achieved at the exit (smaller) base of the trapezium of width f_{entry}.

Fig. 9. Geometrical optics representation of a wedge plasmon mode in a triangular metal wedge with the tip at $y = 0$ (Fig. 1b). The anti-symmetric film plasmon with the wave vector $\mathbf{Q}_1(y)$, representing the wedge plasmon mode, is successively reflected from the tip of the groove and the turning point (caustic); the wave vector of the wedge plasmon mode $q_{wp} = Q_{1x}$.

Figure 1

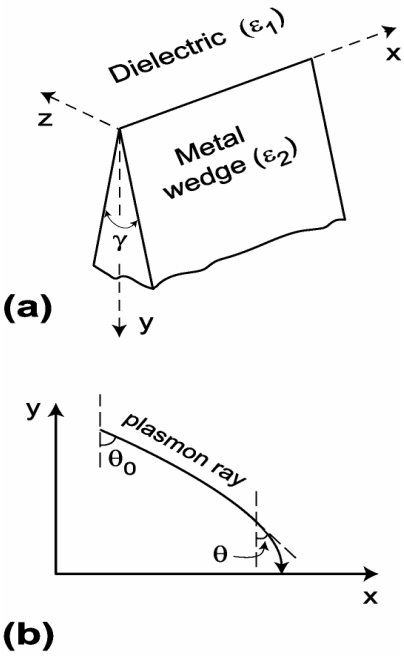
Dielectric (ε_1)
x
z
Metal wedge (ε_2)
γ
y
(a)
y
plasmon ray
θ_0
θ
x
(b)

Figure 2

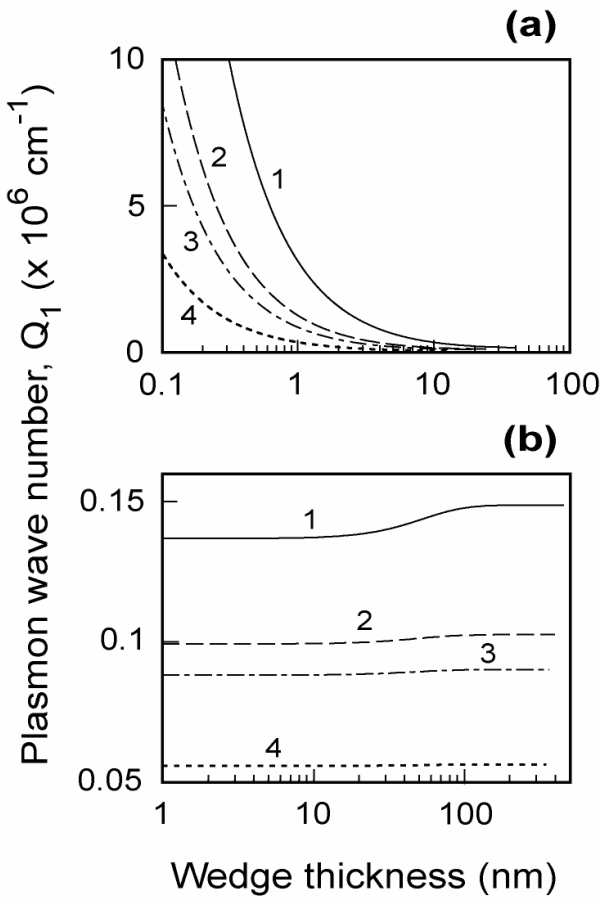
(a)
10
5
0
0.1
1
10
100
1
2
3
4
(b)
0.15
0.1
0.05
1
10
100
1
2
3
4
Plasmon wave number, Q_1 (x 10^6 cm^{-1})
Wedge thickness (nm)

Figure 3

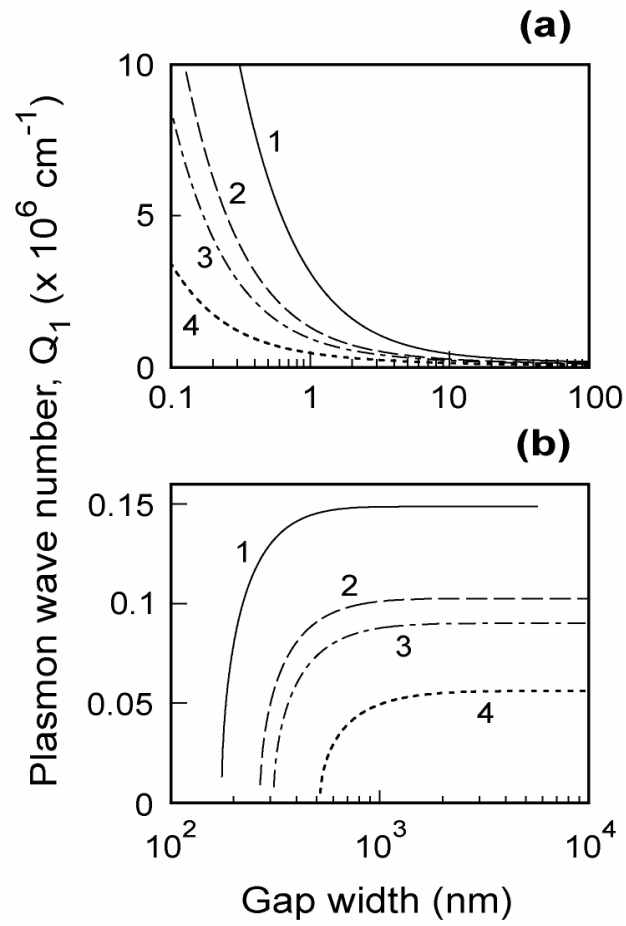
(a)
10
5
0
0.1
1
10
100
1
2
3
4
(b)
0.15
0.1
0.05
0
10^2
10^3
10^4
Plasmon wave number, Q_1 (x 10^6 cm^{-1})
Gap width (nm)

Figure 4

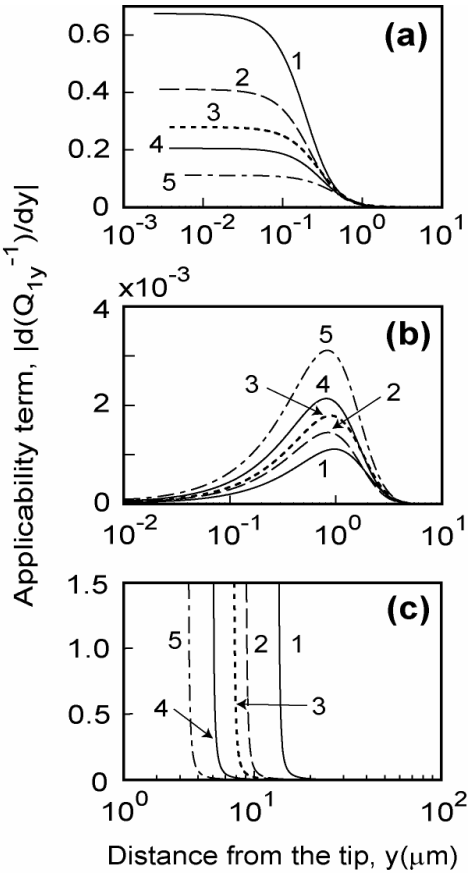
(a)
(b)
(c)
x10^-3
Applicability term, |d(Q1y^-1)/dy|
Distance from the tip, y(μm)
1
2
3
4
5

Figure 5

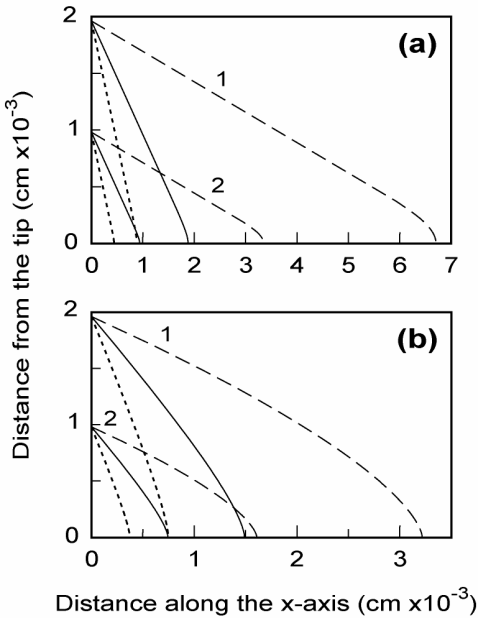
(a)
(b)
1
2
Distance from the tip (cm x10-3)
Distance along the x-axis (cm x10-3)

Figure 6

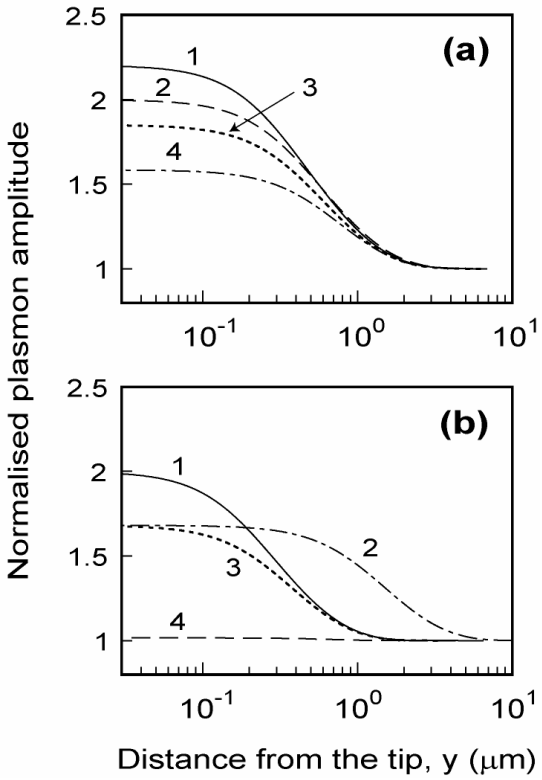
(a)
(b)
1
2
3
4
2.5
2
1.5
1
10^{-1}
10^{0}
10^{1}
Normalised plasmon amplitude
Distance from the tip, y (μm)

Figure 7

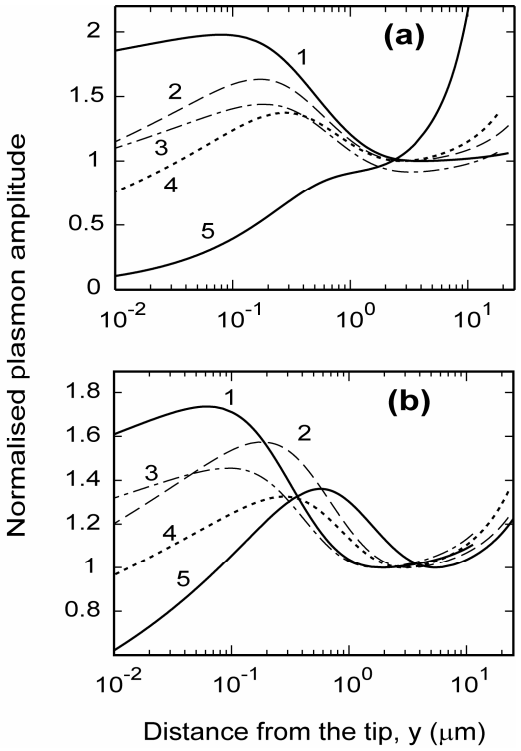
(a)
(b)
1
2
3
4
5
Normalised plasmon amplitude
Distance from the tip, y (μm)

Figure 8

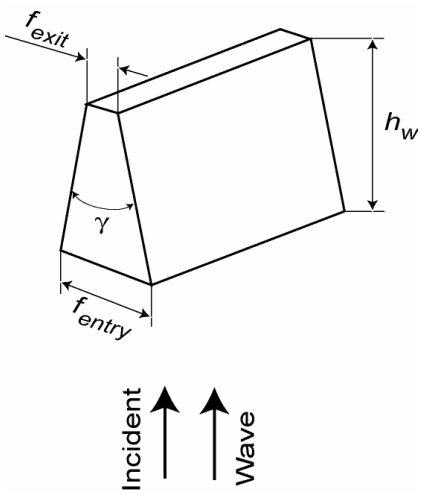

Figure 9